2016

Frost Growth Investigation and Temperature Glide Refrigerants in a Fin-and-Tube Heat Exchanger

Elie Keryakos
CRYOPUR, France / Cnam (Conservatoire National des Arts et Metiers), laboratoire chimie Moléculaire, Génie des Procédés Chimiques et Energétiques (CMGPCE)-EA 7341, France, elie.keryakos@cryopur.com

Joseph Toubassy
CRYOPUR, France, joseph.toubassy@cryopur.com

Denis Clodic
CRYOPUR, France, denis.clodic@cryopur.com

Georges Descombes
Cnam (Conservatoire National des Arts et Metiers), laboratoire chimie Moléculaire, Génie des Procédés Chimiques et Energétiques (CMGPCE)-EA 7341, France, georges.descombes@lecnam.net

Frost Growth Investigation and Temperature Glide Refrigerants in a Fin-and-Tube Heat Exchanger

Elie KERYAKOS[1, 2]*, Joseph TOUBASSY[1], Denis CLODIC[1], Georges DESCOMBES[2]

[1]Cryopur, Ile de France,
Palaiseau, France
(Phone: +33 1 80 38 41 32, Fax : +33 1 80 38 41 31, E-mail : contact@cryopur.com)

[2]Conservatoire National des Arts et Métiers, Laboratoire Chimie Moléculaire, Génie des Procédés Chimiques et Energétiques (CMGPCE) – EA 7341
Paris, France
(Phone: +33 1 40 27 21 77, E-mail: chaire.turbomachines-moteurs@cnam.fr)

ABSTRACT

Bio methane is produced by removing undesirable components such as water vapor, carbon dioxide and other pollutants in a biogas upgrading process. Frosting the water vapor contained in the biogas is one of the dehydration processes used in a biogas upgrading process. In order to simulate a frost layer on a cold plate, many models have been developed. These models are valid for a limited temperature range. In this study, heat and mass transfer equations were used in a numerical approach to model the frost growth and its densification on the external side of a fin-and-tube heat exchanger. The model used in this study is valid for low temperatures from 0 to -65 °C and lower. The evaporation process of temperature glide refrigerants is also modelled. Results show that a decreased heat transfer rate occurred during frost mass growth on fins and rows. During its growth, frost layer thermal conductivity is relatively low leading to a decrease of the cooling load of the heat exchanger. On the other hand, frost layer thickness increases the external surface blockage, leading to higher pressure drop on the external side. This model has been validated by comparing numerical and experimental results.

1. INTRODUCTION

The initiation of frost formation on a fin-and-tube heat exchanger requires specific temperature and humidity conditions. From one hand, the surface temperature of the cold heat exchanger must be lower than the dew point temperature so that water vapor contained in the wet gas begins to condense. From the other hand, the cold surface temperature of the heat exchanger must be lower than the freezing temperature so that frost begins to form on the external side of the heat exchanger. The principal aim of frost formation analysis is to simulate the reduction of heat exchange with the increasing thermal resistance of the frost layer.

Frost formation on cold surfaces have been modeled by several researchers. Most of these models focused on simple geometries such as flat plates, parallel plates and cylinders. O'Neal (1985) was the first to present a theoretical model for frost formation treating it as a porous structure. Using air properties, such as velocity and absolute humidity, his model predicted frost growth and its densification on a cold plate. Sami and Duong (1989) investigated another model for frost thickness growth and its densification, using local properties of frost, with function of time. Lee and al (1997) proposed a mathematical model for frost formation on a cold plate, using molecular diffusion of water vapor and heat generated by the sublimation of water vapor in the frost layer. Other models focused on fin-and-tube heat exchangers geometries used in the refrigeration process for limited temperatures of -15 °C. Oskarsson (1990) developed three models in order to study the performance of a fin-and-tube heat exchanger under dry, wet and frosted conditions. He also tested a six row evaporator of a heat pump under real operating conditions. Rite (1990) studied experimentally heat exchangers integrated in domestic refrigerators. He concluded that the global

heat coefficient is on one hand proportional to air velocity, temperature and humidity. On the other hand, the global heat transfer coefficient decreases with the increasing air side pressure drop. Kondepudi and O'Neal (1991) studied numerically and experimentally the effect of the frost layer on a single row tube heat exchanger with wavy and corrugated fins. Many researchers provided correlations for frost thickness, density and conductivity as functions of air properties. Ogawa (1993) studied fin-and-tube heat exchanger performance used in domestic refrigeration.

The purpose of this study is to investigate frost growth and its effect on the heat exchanger performance as a function of time. The evaporation of gliding temperature refrigerants is also modeled. The numerical model developed will be validated using experimental data extracted from a biogas upgrading pilot called BioGNVAL (2015). Fin-and-tube heat exchangers are used in the dehydration process of this pilot, so that water vapor is removed from biogas by frosting.

2. NUMERICAL MODEL

A numerical model has been developed to investigate frost growth impact on the performance of a fin-and-tube heat exchanger. This model uses the same heat exchanger geometry used in the BioGNVAL pilot. The specifications of the fin-and-tube heat exchanger are listed in Table 1. Both tubes and fins are made from stainless steel 316 L.

Table 1: Heat Exchanger (Evaporator implemented in BioGNVAL) specifications

Parameter	Value
Number of rows, N_p	12
Number of circuits, N_c	3
Fin pitch, S_a (mm)	2
Longitudinal tube spacing, P_l (mm)	34.65
Transversal tube spacing, P_t (mm)	40
Tube outside diameter, d_e (mm)	16.3
Tube thickness, e_t (mm)	1
Fin thickness, e_a (mm)	0.15
Tube length, L_t (mm)	320
Tube material	Stainless Steel 316 L
Fin material	Stainless Steel 316 L

2.1 Introducing the model

The full geometry of the fin-and-tube heat exchanger used in this study is shown in Figure 1. In order to develop a numerical model, the heat exchanger was divided into several control volumes as shown in Figure 2. Each control volume of this heat exchanger is composed of a single row (3 or 2 tubes per row) and the number of associated fins. A blend of refrigerants is flowing into the tubes in a transverse direction with respect to the external flow (biogas). Frost growth on each control volume of the heat exchanger is supposed to be uniform and a one dimensional heat and mass transfer over the heat exchanger is assumed. Outlet properties for both biogas and refrigerant blends of a control volume are used as inlet properties for the next control volume. At each time step, the fin-and-tube heat exchanger geometry is updated (external surface) due to frost growth on the external surfaces. A computer program was written using Visual Basic while REFPROP 9.0 was used to calculate biogas and refrigerant blends properties, such as temperature, pressure, viscosity and density. The same inlet and outlet conditions (temperature and pressure for both flows) of the BioGNVAL pilot are used for this simulation. The computer program starts to run once initial conditions and heat exchanger geometry are provided. Then iterations are made to calculate the frost properties and

thickness, which will lead to modify the heat exchanger geometry so that the new geometry is taken into consideration at the next time step.

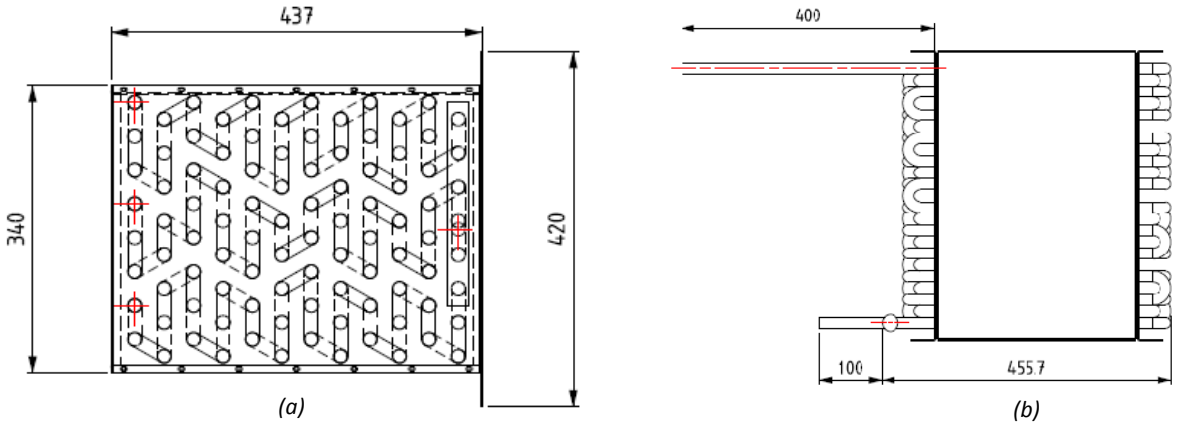

Figure 1: Fin-and-tube heat exchanger geometry implemented in the BioGNVAL pilot: a) Front view b) Face view

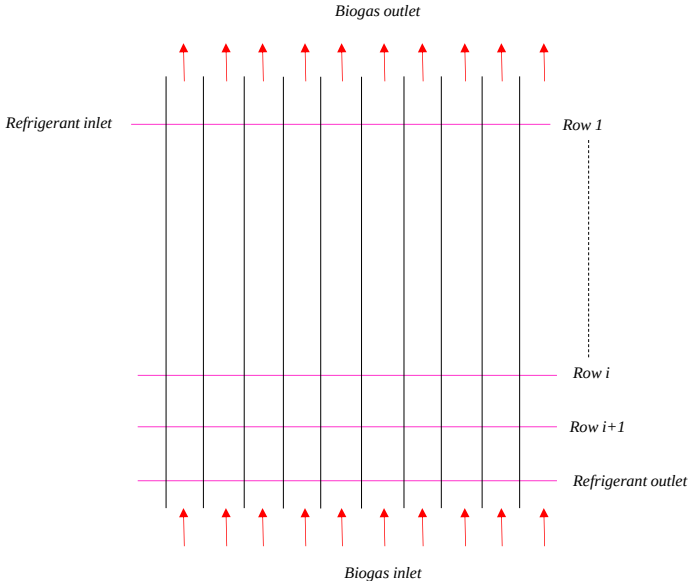

Figure 2: Fin-and-tube heat exchanger control volumes for a single circuit

2.2 Model governing equations

The total heat transfer can be described using refrigerant enthalpies at the inlet and outlet of each row as given in Equation (1). This total heat transferred is the sum of the sensible and latent heat removed from the external flow represented by the biogas.

$$Q_{ech} = \dot{m}_r \cdot \left(i_{outr} - i_{inr}\right) = Q_{sen} + Q_{lat} \tag{1}$$

On one hand, the sensible heat transfer between biogas and frost surface can be expressed as a function of average biogas temperature (T_{avgg}), frost surface temperature (T_{fs}), sensible heat coefficient (h_{sen}) and effective heat transfer area (A_{cv}) relative to each control volume. On the other hand, the sensible heat transfer can be expressed using biogas enthalpies at the inlet and outlet of each control volume. Both expressions are listed in Equation (2).

$$Q_{sen} = h_e \cdot A_{cv} \cdot \left(T_{avgg} - T_{fs}\right) = \dot{m} \cdot \left(i_{ing} - i_{outg}\right) \tag{2}$$

The convective sensible biogas side heat transfer coefficient is calculated using Wang, Chi and Chang correlation (2000) as given in Equation (3).

$$h_e = j \cdot \rho_g \cdot Cp_g \cdot V_g \cdot Pr^{-2/3} \tag{3}$$

Each control volume is associated with an effective heat transfer (A_{cv}), wish is equal to the sum of the external tube surface area (A_t) and the fin surface area (A_a) multiplied by the fin global efficiency (η_a) as given in Equation (4).

$$A_{cv} = A_t + \eta_a A_a = \pi \cdot d_e \cdot L_t + \eta_a \cdot \left[2 \cdot N_{ail} \cdot \left(P_t \cdot P_l - \frac{\pi \cdot d_e^{\,2}}{4} \right) \right] \tag{4}$$

On one hand, the biogas and frost surface latent heat transfer is expressed as a function of average biogas temperature, frost surface temperature, latent heat coefficient (h_{lat}) and effective heat transfer area relative to each control volume. On the other hand, latent heat transfer is expressed using water enthalpy of sublimation (i_{sv}) and the mass of frost captured on each control volume ($\dot{m}_f$). Both expressions are listed in Equation (5).

$$Q_{lat} = h_{lat} \cdot A_{cv} \cdot \left(T_{avgg} - T_{fs} \right) = \dot{m}_f \cdot i_{sv} \tag{5}$$

Using the mass heat coefficient (h_m), the sensible heat coefficient and dimensionless Lewis number (Threlkeld, 1970), the latent biogas side heat coefficient is given by Equation (7).

$$h_m = \frac{h_e}{Cp_g Le^{2/3}} \tag{6}$$

$$h_{lat} = h_m i_{sv} \left(\frac{w_{avg,g} - w_{fs}}{T_{avg,g} - T_{fs}} \right) \tag{6}$$

The fins of the heat exchanger in this study have a rectangular geometry. Their global efficiency is given as a function of fin surface area (A_a), total surface area (A_{tot}) and a dimensionless fin factor (*m*). The global efficiency is given by Equation (8). The dimensionless fin factor is expressed as functions of fin thermal conductivity (λ_a), fin thickness (e_a), frost thermal conductivity (λ_f), frost thickness (δ_f) and both sensible and latent heat coefficients as listed in Equation (9).

$$\eta_a = 1 - \left[1 - \frac{Tanh(mP_l)}{mP_l} \right] \frac{A_a}{A_{tot}} \tag{8}$$

$$m = \left[\frac{2}{\lambda_a \cdot e_a \cdot \left(\frac{1}{h_{sen} + h_{lat}} + \frac{\delta_f}{\lambda_f} \right)} \right]^{0.5} \tag{9}$$

The refrigerant side heat transfer coefficient (h_i) is calculated using Gungor and Winterton correlation (1986). Since the refrigerant blend is evaporating inside of the tubes, the correlation takes into consideration a two-phase fluid by calculating the vapor quality (x_v), vapor density (ρ_v) and liquid density (ρ_l) as shown in Equation (10).

$$h_i = 0.023\left[1+3000Bo^{0.86}+1.12\left(\frac{x_v}{1-x_v}\right)^{0.75}\left(\frac{\rho_v}{\rho_l}\right)^{0.41}\right]\left[\frac{\lambda_l}{d_i}Re^{0.8}\,Pr^{0.4}\right] \quad (10)$$

The overall heat transfer coefficient can be expressed as a function of all the heat transfer coefficient (convective and conduction) calculated for external flow, internal flow and frost layer. This can be expressed by using Equation (11).

$$U = \left[\frac{1}{h_{lat}+h_e}+\frac{Ln\left(\frac{d_e}{d_i}\right)}{2\pi\lambda_t L_t A_{cv}}+\left(\frac{1}{h_i}\right)\left(\frac{1}{S_i L_t A_{cv}}\right)+\frac{\delta_f}{\lambda_f}\right]^{-1} \quad (11)$$

Thus, the total heat transfer can be expressed using the DTLM method which refers to the mean logarithmic temperature difference method given in equation (12).

$$Q_{tot} = UA_{cv}DTLM \quad (12)$$

Biogas side pressure drop is calculated using Kays and London's correlation (1994). Equation (13) is used to represent the external pressure drop.

$$\Delta P_g = \frac{G^2}{2\rho_{in,g}}\left(1+\sigma^2\right)\left(\frac{\rho_{in,g}}{\rho_{out,g}}-1\right)+f\,\frac{A_{tot}}{A_{cv}}\frac{\rho_{in,g}}{\rho_{avg,g}} \quad (13)$$

Where *f*, is the friction factor calculated using the correlation of Wang et al. (2000).

2.3 Frost properties equations

The thermal conductivity of frost (λ_f) is calculated as a function of the frost density (ρ_f) using Lee and Kim correlation (1997), as shown in Equation (14).

$$\lambda_f = 0.132+3.13\cdot10^{-4}\rho_f+1.6\cdot10^{-7}{\rho_f}^2 \quad (14)$$

Using Kandula's correlation (2011), frost surface density (ρ_{fs}) is calculated as a function of frost surface temperature (T_{fs}), Reynolds number (*Re*), tube outlet surface temperature (T_p) and melting temperature of ice (T_m). Frost surface density is expressed using Equation (15).

$$\rho_{fs} = 0.5\rho_{ice}\frac{T_{fs}-T_p}{T_m-T_p}exp\left\{-\left[0.376+1.5\left(1-\frac{T_{fs}-T_p}{T_m-T_p}\right)\right]\left[1-\left(\frac{Re}{Re_c}\right)^{0.5}\right]\right\} \quad (15)$$

The mass of frost captured on each control volume of the heat exchanger is equal to the mass flow of biogas multiplied by the absolute humidity difference between the biogas inlet and outlet flows, as given in Equation (16).

$$\dot{m}_f = \dot{m}_g\left(w_{in,g}-w_{out,g}\right) \quad (16)$$

The mass of frost captured is equal to the sum of two different portions, as given in Equation (17). A portion penetrates into the frost layer thus increasing its density ($\dot{m}_\rho$), while the other portion increases the frost layer thickness ($\dot{m}_\delta$).

$$\dot{m}_f = \dot{m}_\delta+\dot{m}_\rho \quad (17)$$

3. RESULTS AND DISCUSSION

3.1 Frost growth

Figure 3(a) shows the frost thickness growth as a function of time for each row of the heat exchanger. There is a difference of 72 % between frost thickness values comparing second row and final row. At the end of the simulation (after 300 minutes), frost thickness over the second row of the heat exchanger will reach 0.84 mm. This layer is distributed equally on each tube and fin surface of the control volume. Since the control volume takes into consideration half of the fin pitch, an 84 % blockage is reached at the end of the simulation for the second row as shown in Figure 3(b). The frost layer thickness at the end of the simulation for the final row will slightly increase to reach 0.12 mm, which is equal to a 12 % blockage. This percent blockage difference is due to non-uniform mass of frost captured between each control volume. Figure 4 shows the volumetric percentage of water contained in biogas as a function of temperature. This explains clearly the difference between frost thickness values comparing first and final row, since biogas at the final row will reach its lowest temperature.

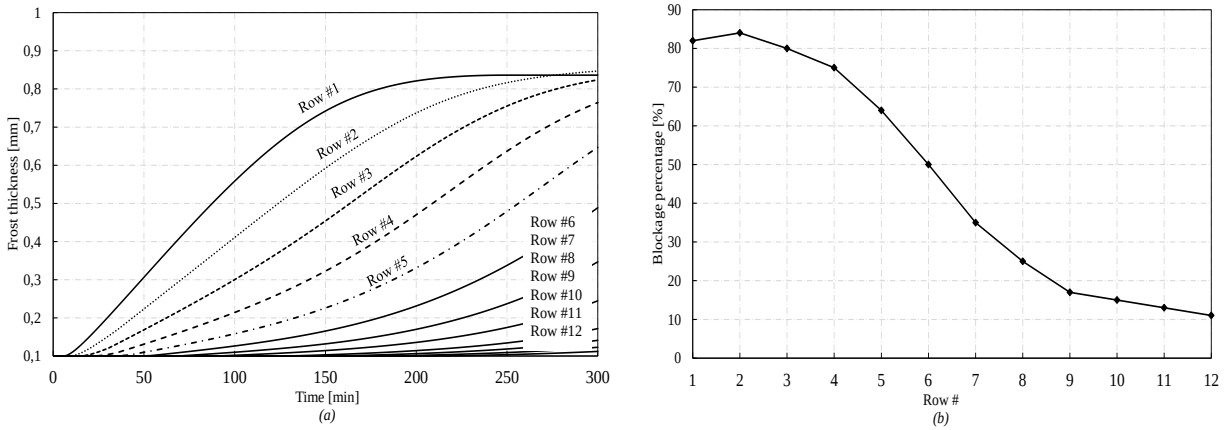

Figure 3: Frost growth on each row of the heat exchanger over time: a) thickness b) percentage of blockage

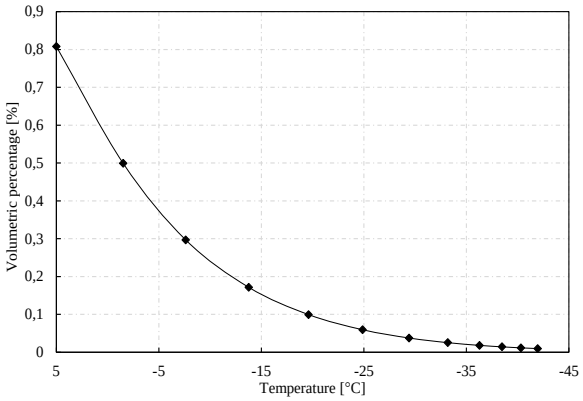

Figure 4: Volumetric percentage of water contained in biogas over temperature

3.2 Heat exchanger performance

On one hand, the heat exchanger performance is represented by its cooling capacity. The cooling capacity controls the lowest temperature reached by the external flow. On the other hand, since frost is growing during cooling, the external pressure drop affects also the heat exchanger performance and the frosting cycle duration. Figure 5 shows the cooling capacity decrease and the external pressure drop increase over time. Increasing frost thickness tends to decrease total heat transferred and to increase external pressure drop. The external pressure drop is increased due to passage reduction, while heat transferred or cooling capacity is decreased due to the high thermal resistance of the frost layer. At the end of the simulation (after 300 minutes), cooling capacity will decrease by 14 %, while pressure drop will be 150 times greater (40000 Pa) than its initial value (280 Pa).

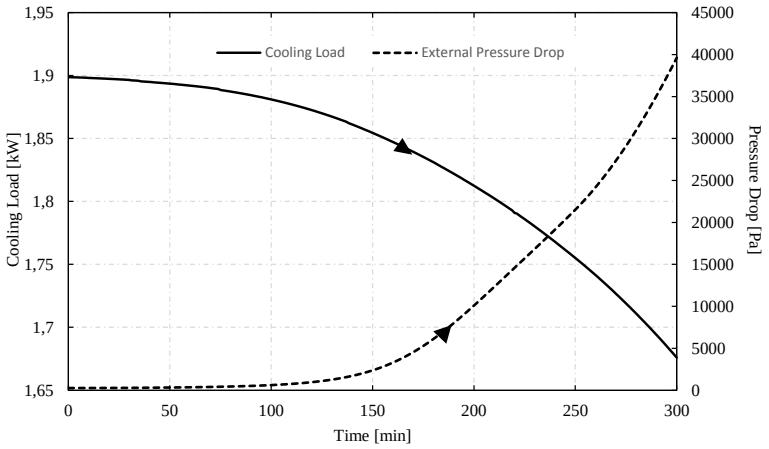

Figure 5: Cooling load loss and external pressure drop over time

To simulate the effect of the evaporation and the temperature glide phenomenon on the performance of the heat exchanger, two refrigerant blends where compared. Figure 6 shows temperature variations for biogas and for (a) blend X and (b) blend Y, at each row of the heat exchanger at the beginning of the simulation. Figure 6(a) shows that temperature difference between biogas and blend X is slightly increasing from rows 12 to 1 while blend X is evaporating with a high temperature glide. Figure 6(b) shows that temperature difference between biogas and blend Y is considerably increasing from rows 12 to 1 while blend Y is evaporating at a constant temperature with a slight superheating degree at the final row. In this case, blend X is classified as a non-azeotropic mixture (with temperature glide), while blend Y is classified as azeotropic mixture (no temperature glide). The comparison was made using the same mass flow and inlet temperature for both blends. While comparing biogas outlet temperature for both cases, it was found that using blend X instead of blend Y increases the heat exchanger performance by about 30 %.

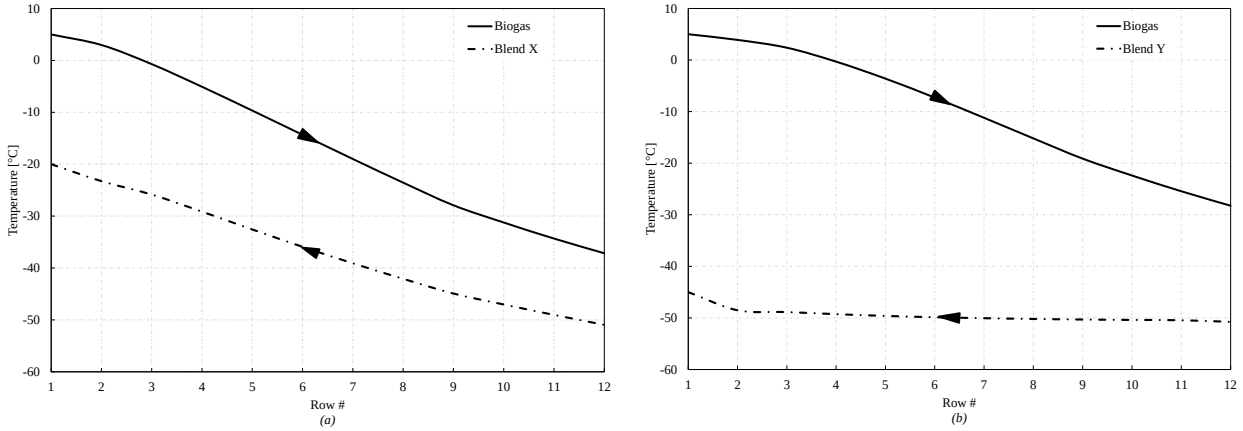

Figure 6: Temperature variations and evaporation of refrigerant blends at each row of the heat exchanger: a) blend X, b) blend Y

3.3 Data Comparison

In order to validate the numerical model developed in this study, experimental data were collected from the biogas upgrading pilot. One of the data collected is the biogas outlet temperature as a function of time. Figure 7 compares biogas outlet temperature for both experimental and calculated data. The maximum error found was 13 % while comparing both temperature curves. The same initial conditions such as inlet temperature and pressure for both flows, operating the BioGNVAL pilot, were used to perform this comparison.

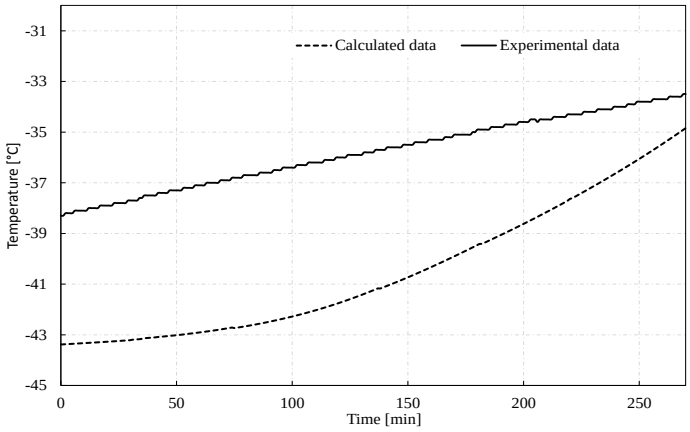

Figure 7: Biogas outlet temperature comparison between experimental and calculated data

4. CONCLUSIONS

In this study the investigation of frost growth on the cold surfaces of a stainless steel fin-and-tube heat exchanger was validated using a numerical model. The heat exchanger performance is affected during frost growth on its surfaces. This performance is represented by the cooling load capacity, which decreases as function of time due to the high thermal resistance of frost. The external pressure drop also increased due to the increased percentage of blockage wish generated a reduction in the external flow passage surface. Using a high temperature glide refrigerant blend tends to increase the heat exchanger performance.

NOMENCLATURE

A	surface area	(m²)
Bo	boiling number	(-)
Cp	isobaric heat capacity	(kJ/kg K)
d	diameter	(mm)
e	thickness	(mm)
f	friction factor	(-)
G	maximum mass flux	(kg/m² s)
h_e	convective biogas side heat transfer coefficient	(W/m² K)
h_i	convective refrigerant side heat transfer coefficient	(W/m² K)
h_{lat}	latent heat transfer coefficient	(W/m² K)
h_m	mass transfer coefficient	(kg/m² s)
i	enthalpy	(kJ/kg)
i_{sv}	latent heat of sublimation	(kJ/kg)
Le	lewis number	(-)
L_t	tube length	(mm)
m	dimensionless fin factor	(-)
$\dot{m}$	mass flow rate	(kg/s)
N_c	number of circuits	(-)
N_p	number of rows	(-)
P_l	longitudinal tube spacing	(mm)
Pr	prandtl number	(-)
P_t	transversal tube spacing	(mm)
Q	heat transferred	(W)

Re	reynols number	(-)
S_a	fin pitch	(mm)
T	temperature	(°C)
t	time	(min)
U	global heat transfer coefficient	(W/m² K)
w	absolute humidity	(kg/kg)
x	quality	(-)

Greek Symbols

ρ	density	(kg/m³)
η_a	fin global efficiency	(-)
δ_f	frost thickness	(mm)
σ	ratio of minimum flow area over face area	(-)
λ	thermal conductivity	(W/m K)

Subscripts

a	fin	*p*	tube surface
avg	average	*r*	refrigerant
c	critical	*sens*	sensible
f	frost	*t*	tube
fs	frost surface	*v*	vapor
g	biogas		
in	inlet		
l	liquid		
lat	latent		
m	melting		
out	outlet		

REFERENCES

Cryo Pur, (2015). Valorize biogas with bio-LNG and bioCO2. *From http://www.cryopur.com/.*

Gungor, K.E., Winterton, R.H.S. (1986). A general correlation for flow boiling in tubes and annuli. *Int. J. Heat and Mass Transfer, 29*(3), 351–358.

Kandula, M. (2011). Frost growth and densification in laminar flow over flat surfaces. . *Int. J. Heat and Mass Transfer, 54*(15), 3719–3731.

Kays, W.M., London, A.L. (1994). *Compact heat exchangers (3rd edition).* Malabar, FL: Krieger Publishing Company.

Kondepudi, S.N., O'Neal, D.L. (1991). Frosting performance of tube fin heat exchangers with wavy and corrugated fins. *Experimental Thermal and Fluid Science, 4*(5), 613–618.

Lee, K.S., Kim, W.S., Lee, T.H. (1997). A one dimensional model for frost formation on a cold flat surface. *Int. J. Heat and Mass Transfer, 40*(18), 4359–4365.

Ogawa, K., Tanaka, N., Takeshita, M. (1993). Performance improvement of plate fin-and-tube heat exchanger under frosting conditions. *ASHRAE conferences: Proceeding of the conference by ASHRAE* (2–4). Chicago, IL, USA.

O'Neal, D.L., Tree, D.R. (1985). A review of frost formation in simple geometries. *ASHRAE Transactions, 91*(2), 267–281.

Oskarsson, S.P., Krakow, K.I., Lin, S. (1990). Evaporation models for operation with dry, wet and frosted surfaces part 1 & 2: heat transfer and fluid theory & evaporator models and verification. *ASHRAE Transactions, 96*(1), 373–392.

Rite, R.W. (1990). The effect of frosting on the performance of domestic refrigerator-freezer finned tube evaporator coils. *Master thesis*, Univerisity of Illinois, USA.

Sami, S.M., Duong, T. (1989). Mass and heat transfer during frost growth. *ASHRAE Transactions, 91*(1), 158–165.

Threlkeld J. (1970). *Thermal environmental engineering (2nd edition).* Englewood Cliffs, NJ: Prentice Hall Book Co.

Wang, C.C., Chi, K.Y., Chang, C.J. (2000). Heat transfer and friction characteristics of plain fin-and-tube heat exchangers, part II: Correlation. *Int. J. Heat Mass Transfer, 43*(15), 2693–2700.

ACKNOWLEDGEMENT

This work was supported by Cryopur. We thank Amélie Danlos for her comments that greatly improved the manuscript.